Synthesis and Ultrafast Study of Cysteine- and Glutathione-Capped Ag_2S Semiconductor Colloidal Nanoparticles

Michael C. Brelle,[†] Jin Z. Zhang,*[,†] Liem Nguyen,[‡] and Rajesh K. Mehra*[,§]

Department of Chemistry, University of California, Santa Cruz, California 95064, Department of Biochemistry, University of California, Riverside, California 92521, and Department of Environmental Toxicology, University of California, Riverside, California 92521

Received: June 17, 1999; In Final Form: August 16, 1999

A new synthetic method has been developed for preparing silver sulfide, Ag_2S, nanoparticles capped with cysteine or glutathione. The average particle diameter has been determined to be around 9 nm using transmission electron microscopy. The ground-state electronic absorption spectra of the Ag_2S nanoparticles show a continuous increase in absorption cross section toward shorter wavelengths starting from the red (600−800 nm). Ultrafast dynamics of photoinduced electrons in these nanoparticles have been measured using femtosecond transient absorption/bleach spectroscopy. In most cases studied, the early time transient profiles feature a pulse-width limited (<150 fs) rise followed by a fast decay (750 fs) and a slower rise (4.5 ps). The signal has contribution from both transient absorption and transient bleach. On longer time scales, three (Cys-1, Cys-2, and GSH-2) of the four samples studied show a recovery with 4.5 ps time constant that goes above the baseline and then decays gradually toward the baseline with a time constant of >1 ns. One sample (GSH-1) shows a bleach recovery that gradually approaches the baseline with a similar time constant (>1 ns) following the fast 4.5 ps rise. An interesting power dependence was observed for all the samples: the transient absorption contribution becomes more dominant over bleach with increasing excitation intensity. A simple four-state kinetic model developed to account for the main features of the dynamics suggests that initial photoexcitation populates the conduction band and depletes the valence band within the laser pulse (<150 fs). The conduction band electrons are first trapped in shallow trap states with a time constant of 500 fs and then further trapped into deep traps with a constant of 4 ps. The deep trapped electrons finally recombine with the hole with a time constant of >1 ns. This model suggests that the difference in dynamics observed between the different samples is due to different absorption cross sections of deep trap states. The observed excitation intensity dependence of the dynamics is attributed to shallow trap state saturation at high intensities.

Introduction

It had been known for a long time that microorganisms such as selected bacteria and yeasts formed metal sulfides in response to metal ion stress.[1,2] However, it was discovered only recently that in many instances the metal sulfides formed in microbial systems exhibited properties of nanocrystalline semiconductors.[3,4] Detailed in vivo studies revealed that the exposure of yeasts *Candida glabrata* and *Schizosaccharomyces pombe* to Cd resulted in the formation of nanocrystalline CdS particles that were capped with peptides such as glutathione and its derivative phytochelatins with the general structure (γ-Glu−Cys)$_n$Gly.[3−6] These studies indeed provided the first clue for utilizing thiolate amino acids for the nucleation of nanoparticles. The formation of CdS nanocrystallites occurred more readily in stationary phase cultures that produced inorganic sulfide. Biological studies also established the existence of specific genetic pathways for the in vivo formation of glutathione- or phytochelatin-capped nanocrystalline CdS.[7] However, in vitro studies established that such genetic pathways are dispensable for the synthesis of metal sulfide nanocrystalline semiconductor particles.[8−13]

The intrinsic metal-chelating properties of cysteine and glutathione enables them to form high-affinity metal−ligand clusters. These preformed metal−biomolecule complexes can then serve as excellent matrixes due to the ability of the corresponding biomolecule to effectively compete for metal binding sites and thus restrict the incorporation of inorganic sulfide during the process of metal-sulfide nucleation. Indeed, the thiol-containing amino acids have now been shown to be excellent nucleating agents for the synthesis of CdS and ZnS nanoparticles.[9−13] The significance of nanocrystalline metal sulfides in metal detoxification and their utility in photocatalytic degradation of environmental contaminants have already been established.[9−14]

The ability of cysteine and glutathione to dictate the formation of metal-sulfide nanoparticles led us to use these thiol-containing biomolecules to mediate the formation of Ag_2S nanoparticles. Attempts to synthesize colloidal Ag_2S nanoparticles have been for the most part very difficult owing to their tendency to aggregate into bulk. One solution reported was to synthesize Ag_2S nanoparticles in reverse micelles.[15] In this paper, we report a simple, efficient, and reproducible route to the synthesis of colloidal Ag_2S capped with glutathione and cysteine. Furthermore, the use of bifunctional capping agents such as mercapto-

* Corresponding authors.
[†] Department of Chemistry, University of California, Santa Cruz, California.
[‡] Department of Biochemistry, University of California, Riverside, California.
[§] Department of Environmental Toxicology, University of California, Riverside, California.

10.1021/jp991999j CCC: $18.00
Published on Web 09/11/1999

carboxylic acids[16] or thiolate-amino acids confer additional advantages in that the surface states of these molecules may be controlled with solution pH, thus providing a convenient mechanism for manipulating surface states of bifunctionally capped nanoparticles.[9,16] Ag_2S nanoparticles capped with biomolecules also provide the opportunity to study interaction between nanoparticles and biomolecules and are promising for applications including biological fluorescence imaging, as shown with CdS nanoparticles.[17,18] Ag_2S nanoparticles coated with dodecanethiol have been found to form self-assembled large domain hexagonal 2-dimensional layers and highly ordered face-centered cubic 3-dimensional structures.[15,19,20] Silver sulfide thin films with stoichiometric compositions containing excess silver have shown great promise for photoimaging and photodetection in the IR region.[21]

Silver sulfide nanoparticles represent an interesting class of semiconductor nanoparticles with unique properties compared to bulk or isolated atoms and molecules due to quantum size confinement and an extremely large surface-to-volume ratio.[22−28] They are excellent systems for studying interfacial properties of charge carriers, as has been demonstrated in a number of systems such as TiO_2[29−36] and silver halides.[37−39] Time-resolved laser techniques are particularly useful in determining dynamic properties of charge carriers in semiconductor nanoparticles. Femtosecond studies have been performed on core/shell structured nanoparticles of AgI/Ag_2S and AgBr/Ag_2S, and a dependence of the charge carrier dynamics on the ratio of silver sulfide:silver halide has been found.[40] However, to date, no dynamic studies have been reported on neat silver sulfide nanoparticles.

Beyond the new synthetic methods for making Ag_2S nanoparticles, this paper will introduce the first femtosecond dynamic study of Ag_2S nanoparticles. The observed signal showed interesting features not seen in other semiconductor nanoparticle systems previously. Following initial photoexcitation at low excitation intensity, a short-lived transient absorption signal was observed which decayed with a time constant of 750 fs into a transient bleach signal. Two different recovery schemes were observed depending on the sample. In all but one sample, the transient bleach signal recovered to and beyond the baseline and turned into a transient absorption signal with a time constant of 4.5 ps, followed by a slow decay back to baseline on the time scale of >1 ns. One particular sample, however, did not show the fast bleach recovery but rather maintained a long-lived bleach signal which recovered with a time constant of >1 ns. Interestingly, at higher excitation intensities, the signal remained in the transient absorption regime and transient bleach signal became insignificant. This power dependence is attributed to shallow trap state saturation that results in an increase in excited-state absorption and decrease in ground-state bleach. By applying a four-state kinetic model, it was determined that this difference observed between the samples was related to the nature of the deep traps involved in the electronic relaxation processes. The change in absorption cross section of the deep trap states, which affects the observed signal, depends on both stoichiometric ratio of silver:sulfide:capping material and the capping material itself.

Experimental Section

The synthesis of glutathione- (GSH-) and cysteine-capped Ag_2S nanoparticles involves a two-step procedure. In the first step, metal−thiolate complexes were stoichiometrically formed utilizing a thiol to Ag(I) molar ratio of 2:1. Ag(I) in the form of silver acetate (0.1 M in 1% trifluoroacetic acid) was titrated with concomitant stirring into a deaerated Tris buffer (1M Tris-hydroxymethyl aminomethane, pH 10.5) solution containing dissolved glutathione or cysteine to form the corresponding Ag−cysteine or Ag−glutathione clusters. The nucleation of Ag(I) ions and sulfide (S^{2-}) was then achieved by stoichiometrically titrating various amounts of inorganic sulfide (Na_2S) into the corresponding preformed Ag−thiolate complexes. In the present study, sulfide additions were performed to obtain initial sulfide:Ag(I) ratios of 0.5:1.0 (Cys-1 and GSH-1) and 1:1 (Cys-2 and GSH-2). It should be pointed out that as the sulfide:Ag(I) ratio increases the capping material:Ag(I) ratio decreases, since the capping material is replaced by the sulfide ions. Thus, Cys-2 and GSH-2 are expected to have a lower ratio of capping materials than Cys-1 and GSH-1. All additions were performed with intense vortexing. Following the nucleation of Ag_2S nanoparticles, the samples were immediately sealed, followed by incubation at room temperature for 30 min. After the incubation period, the samples were thoroughly purged with nitrogen gas to remove unreacted sulfide. The resulting Ag_2S colloidal nanoparticles were subsequently subjected to a size-selective precipitation procedure to limit particle size polydispersity. To selectively isolate a given population of Ag_2S, a 1/10 (100 μL/mL) volume aliquot of 3 M sodium acetate, pH 6, was added to the sample under vigorous stirring conditions followed by dropwise addition of 100% cold ethanol. Ethanol was continuously added until a dark precipitate appeared. The resulting cloudy sample was thereafter centrifuged using a Beckman Model TJ-6 at 3000 rpm for 10 min. The supernatant was discarded, and the resultant pellet containing Ag_2S nanoparticles was dissolved in deaerated 1 M Tris buffer or water, depending on the application. The size selective precipitation procedure was repeated up to 3 times to achieve maximal particle size monodispersity and uniform chemical composition.

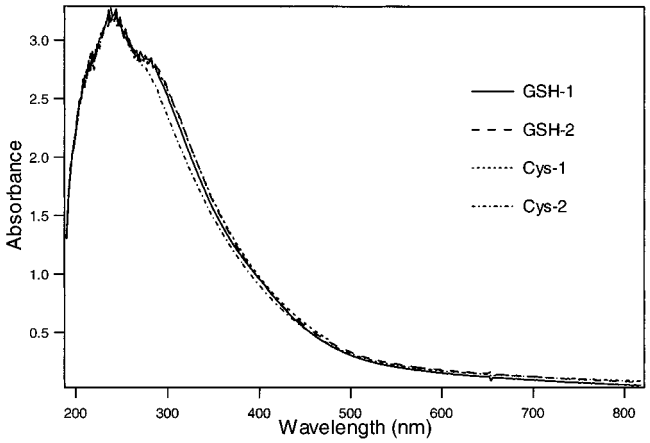

Figure 1. Electronic absorption spectra of silver sulfide nanoparticles in water. Solid: GSH-1; dashed: GSH-2; dotted: Cys-1; dot/dash: Cys-2.

The concentrated samples were prepared for kinetic studies by diluting with milli-Q water to obtain an optical density of 1 at 390 nm. The ground-state absorption spectra were taken on an HP-8452A UV−visible spectrometer. The transmission electron microscopy (TEM) sample was prepared by depositing a droplet of the solution onto a carbon film supported by copper grids. Low-resolution TEM images were taken on a JEOL-100 CX electron microscope. High-resolution (HR) TEM images were recorded at 200 kV using a JEOL 2002 and a Hitachi HF-2000 electron microscope. A small objective aperture was used to enhance the diffraction contrast.

The dynamics measurements were performed using a pump−probe scheme with a regeneratively amplified, mode-locked

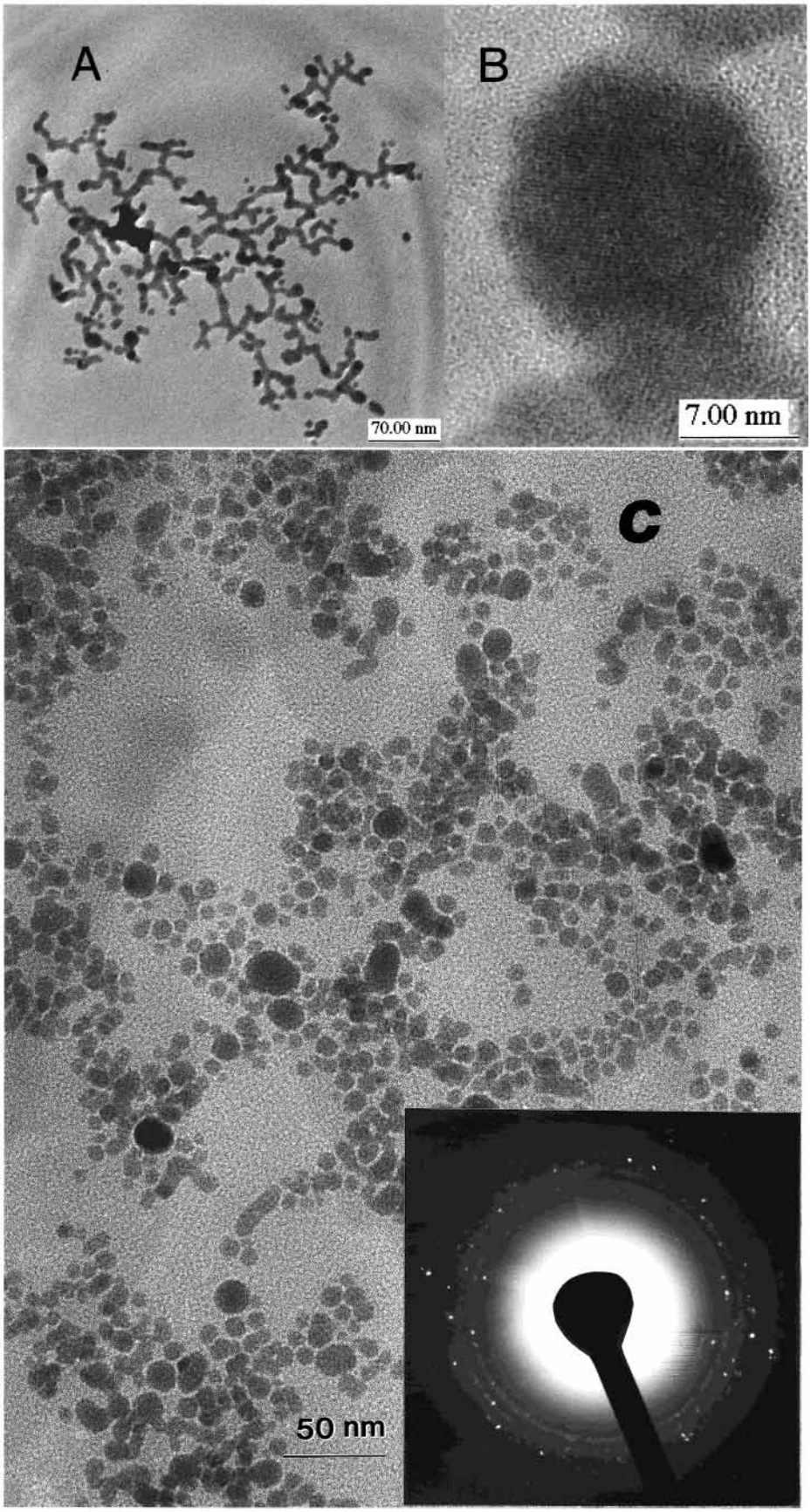

Figure 2. High-resolution TEM photographs of sample GSH-1: (A) and (B) were measured on a JEOL 2002 electron microscope. (C) was recorded on a Hitachi HF-2000 electron microscope. The inset of (C) is the electron diffraction pattern, indicating crystallinity of the Ag_2S nanoparticles. The average size was ~9 nm with a standard deviation of ~25% of the average size.

femtosecond Ti-sapphire laser.[41] Pulses of 40 fs duration with 5 nJ/pulse energy at a repetition rate of 100 MHz were generated and amplified in a Ti-sapphire regenerative amplifier using chirped-pulse amplification. The final output pulses obtained

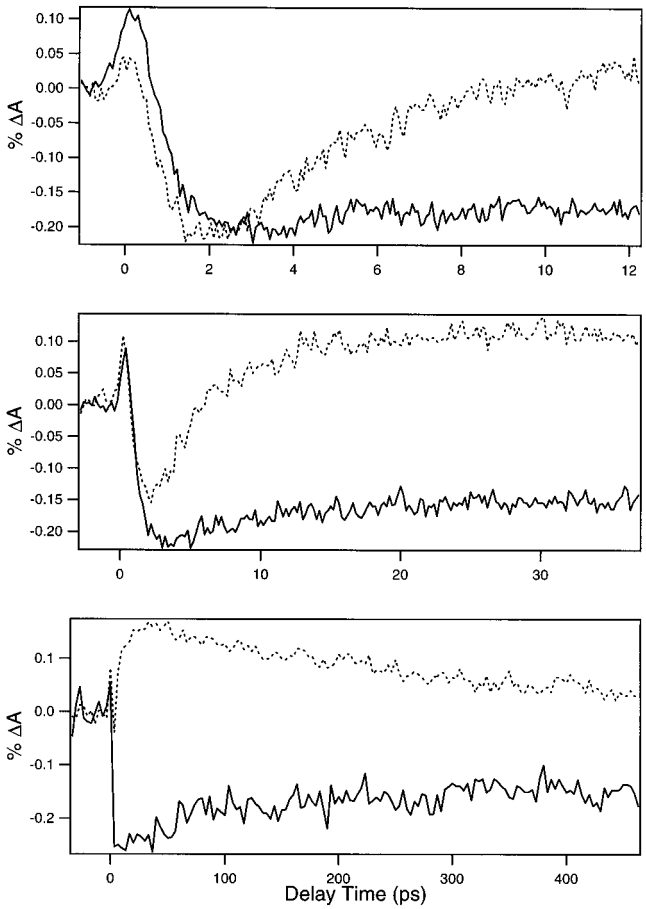

Figure 3. Time evolution of photoinduced electrons in GSH-1 (solid) and Cys-1 (dotted) probed at 790 nm following excitation at 390 nm. Three different time scales are shown for both visualization and data analysis.

were typically 150 fs with pulse energy of 350 μJ, centered at 780 nm at 1 kHz. The amplified output was doubled in a 1 mm KDP crystal to generate 30 μJ/pulse of 390 nm light, which was used as a pump source to excite the nanoparticles contained in a quartz cell with a 1 cm optical path length. The remaining fundamental was focused into quartz to generate a white light continuum and the desired probe wavelength was selected using an interference band-pass filter. The probe beam was split into a signal and reference, which were detected by two photodiodes and processed by a computer-controlled, gated integrator. Pulse-to-pulse fluctuation was eliminated by dividing the signal by the reference for each laser shot. The time delay between pump and probe was controlled by a translation stage. The pump and probe beams were focused with a 10 cm focal length lens and cross overlapped over a spot size of 1 mm^2 in the sample before the focal point. The pump power was attenuated to such a level ($\sim$15 μJ/pulse) that there was no signal observed from the pure solvent due to multiphoton ionization.

Results

The ground-state electronic absorption spectra of several samples of cysteine- and GSH-capped Ag_2S nanoparticles are shown in Figure 1. All the spectra are virtually identical and show a gradual increase in absorption toward shorter wavelengths with no discrete peaks. The band gap of bulk silver sulfide is 1 eV (1240 nm).[42] The apparent large blue shift of the observed absorption indicates that the nanoparticles are within the quantum confinement regime, in which a blue shift in absorption is often expected with decreasing particle size.

Of particular importance is to note that there is a small amount of ground-state absorption in the near-IR region. This is the region where the probe wavelengths are used for the dynamics studies. Therefore, it is expected that this ground-state absorption will contribute to the observed transient signal as a bleach due to ground-state depletion upon photoexcitation. This will be important when assigning the observed dynamics signal and related relaxation processes.

No emission was detected at room temperature for any of the samples, indicating that the major relaxation pathways of the excited-state charge carriers are nonradiative.

Particle size was determined by both low- and high-resolution TEM measurements. Low-resolution TEM seems to show a larger size, probably due to limited spatial resolution. Some representative HRTEM micrographs for sample GSH-1 are shown in Figure 2. Figure 2A seems to show aggregates of the Ag_2S nanoparticles, which are most likely caused by interaction of the capping biomolecules. There appears to be much less aggregates in Figure 2C, probably due to a lower particle concentration. Based on HRTEM, the mean particle diameter was found to be 9 nm with size distribution of $\sim$25% of the average size (standard deviation). The HRTEM picture (Figure 2B) and the electron diffraction pattern (inset of Figure 2C) clearly show crystallinity of the particles. The lattice constants calculated from Figure 2B are consistent with those of bulk Ag_2S.[42] The average size and size distribution are similar for other samples studied.

Figure 3 shows the time evolution of the photoinduced electrons of two Ag_2S samples capped with cysteine (Cys-1) and GSH (GSH-1), respectively, probed at 790 nm following photoexcitation at 390 nm on three different time scales. Both samples show similar dynamics during the first 2 ps after photoexcitation: a fast pulse-width limited ($<$150 fs) rise, leading to a positive signal or transient absorption, followed by a fast 750($\pm$100) fs decay. The decay actually goes below the baseline and leads to a negative signal or transient bleach that recovers on longer time scales. The recovery on long time scales is quite different between the two samples. Sample Cys-1 shows a fast recovery of the bleach signal back to the transient absorption regime with a time constant of 4.5($\pm$0.5) ps. This second transient absorption feature then decays with a time constant of $>$1($\pm$0.2) ns. Sample GSH-1 shows a similar 4.5 ps bleach recovery. However, the amplitude of this fast recovery is much smaller and the subsequent recovery gradually approaches the baseline with a time constant of $>$1 ns but never crosses the baseline as in the case of Cys-1.

Figure 4 shows time profiles of photoinduced electrons for two samples: (A) Cys-2 and (B) GSH-1 on a short (12 ps) time scale at three different probe wavelengths, 720, 790, and 900 nm. The overall transient absorption and bleach features are very similar to those in Figure 3 and similar among the three probe wavelengths. However, it can be seen that the amplitude of the initial transient absorption signal increases as the probe wavelength moves toward the red. This could be due to an increase of absorption cross section of the photoinduced electrons with increasing wavelength. However, it could also be due to less transient bleach contribution to the signal with increasing wavelength, since the amplitude of the bleach is expected to decrease due to smaller ground-state absorption cross section at longer wavelength. Within the signal/noise ratio, the rise and decay time constants do not change upon changing probe wavelengths.

Figure 5 shows the time evolution of the transient absorption/bleach profiles of GSH-1 at two different excitation intensities and three different probe wavelengths, (A) 790 nm, (B) 820

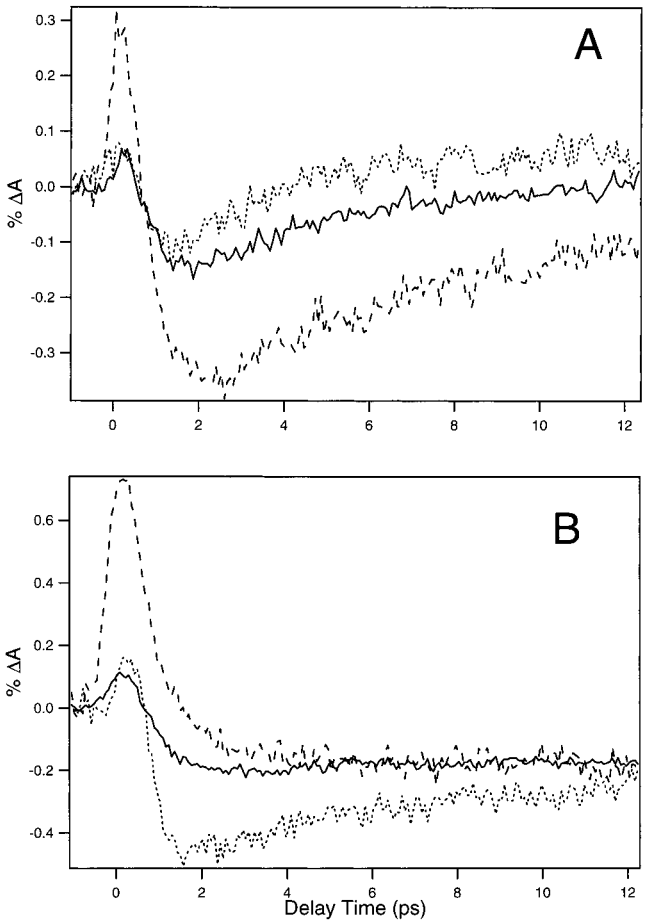

Figure 4. Probe wavelength dependence of the electron relaxation dynamics of Cys-2 (A) and GSH-1 (B). Dotted: 720 nm; solid: 790 nm; dashed: 900 nm.

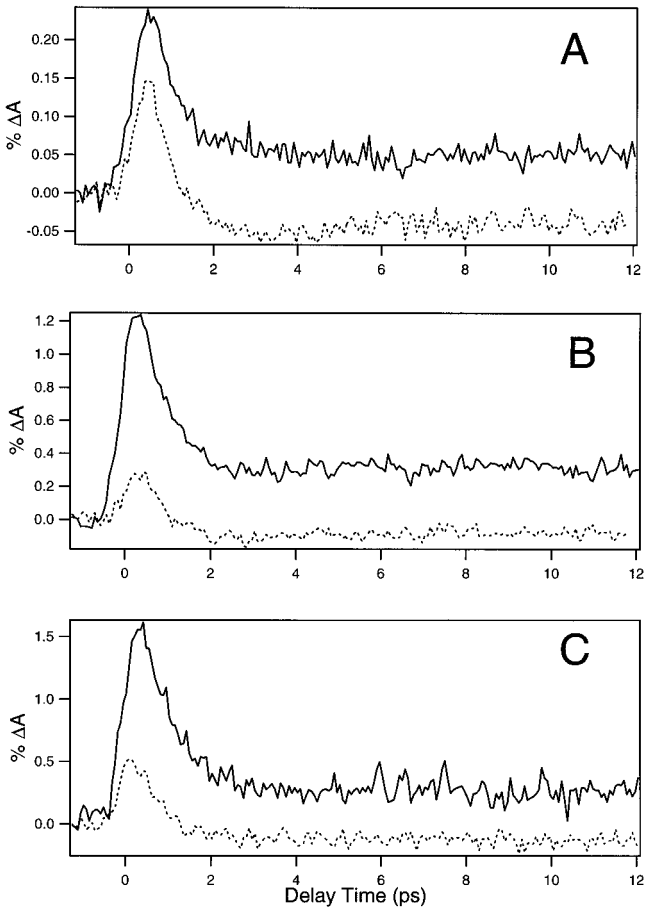

Figure 5. Probe wavelength and excitation intensity dependence of the electron relaxation dynamics of GSH-1. Solid lines represent 7 μJ/pulse, dotted lines represent 3.5 μJ/pulse. Probe wavelengths: 790 nm (A), 820 nm (B), 900 nm (C).

nm, and (C) 900 nm. At low excitation intensity (dashed lines), the time profiles are similar to those shown in Figure 3 (GSH-1). The dynamics feature a pulse-width limited (<150 fs) rise and a 750 fs decay followed by a slow rise (>1 ns) which recovers toward the baseline. In this case, the amplitude of the 4.5 ps rise is very small and almost unnoticeable. As the excitation intensity was increased, the time profile changed dramatically. First of all, the initial transient absorption signal increases in amplitude, as one may expect. Second and perhaps more interesting, the signal stayed positive as transient absorption and never goes below the baseline. This indicates that the transient absorption is predominant over bleach at higher excitation intensities. This trend has been observed for a series of excitation intensities. Possible explanations for this observation will be given in the Discussion Section.

Figure 6 shows the time evolution of the transient absorption/bleach profiles of GSH-2 at two different excitation intensities and three different probe wavelengths, (A) 790 nm, (B) 850 nm, and (C) 900 nm. At low excitation intensity (dashed lines), the dynamics show a pulse-width limited (<150 fs) rise and a fast decay with a 750 fs time constant that leads the signal to negative or bleach. The bleach then recovers with a time constant of 4.5 ps toward the baseline. At high intensity (solid lines), the transient absorption becomes more dominant over transient bleach on this short time scale studied, similar to that observed for GSH-1 in Figure 5. The same power-dependent behavior, i.e., increase in transient absorption contribution over bleach, has been observed for the two cysteine samples as well (data not shown).

Discussion

Ground-State Electronic Absorption. The absorption spectrum of Ag_2S nanoparticles shown in Figure 1 is substantially blue shifted with respect to that of the bulk. A previous study of silver sulfide nanoparticles synthesized in reverse micelles also found a large blue shift in absorption relative to that of bulk but no indication of dependence on particle size in the range of 3−6 nm.[19] The lack of size dependence was not explained and could be due to polydispersity of particle sizes or indirect band gap transitions. Since the Bohr exciton radius for Ag_2S has not been reported, to our best knowledge, and the reduced mass of the electron and hole for Ag_2S cannot seem to be found either, we cannot calculate its Bohr exciton radius. However, since we observed little ground-state absorption in the near-IR, it appears likely that the Ag_2S particles are in or near the quantum-confined regime. Additionally, it is known that significant blue shift of absorption can be observed in some nanoparticles, e.g., PbI_2, even when their size is larger than the Bohr exciton radius but smaller than about 3 times the Bohr radius, which is considered the weakly quantum-confined regime.[43]

The strong similarity between the spectra of cysteine-capped and GSH-capped samples studied here indicates that the capping material has little influence on the ground-state absorption spectrum. The absence of discrete features, e.g., sharp excitonic absorption peaks, for a semiconductor system usually indicates an indirect band gap transition. Silver sulfide is known to have both direct and indirect transitions in the visible and red

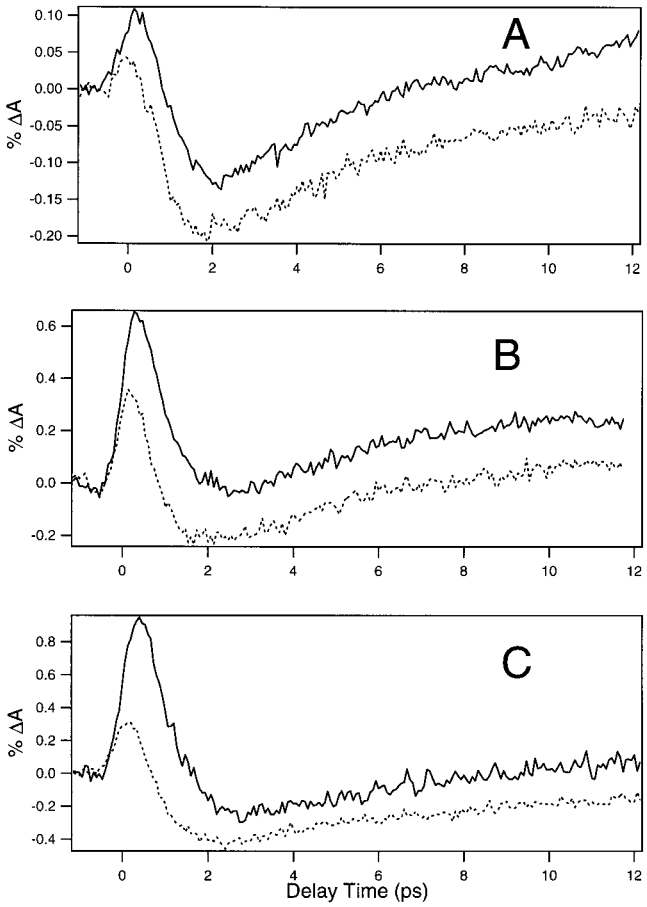

Figure 6. Probe wavelength and excitation intensity dependence of the electron relaxation dynamics of GSH-2. Solid line represents 6.5 μJ/pulse, dotted line represents 3.2 μJ/pulse. Probe wavelengths 790 nm (A), 850 nm (B), and 900 nm (C).

regime.[42] The lack of a strong absorption onset characteristic of direct band gap transitions seems to indicate that the nanoparticles prepared may be indirect band gap semiconductors. The absence of detectable fluorescence at room temperature would seem to be consistent with an indirect band gap transition in these Ag_2S nanoparticles.

Assignment of Transient Signals. As stated in the Results Section, the observed signals are clearly due to a combination of two processes, excited-state electron absorption (positive signal) and ground-state electron depletion or bleaching (negative signal). Since the ground-state absorbs the probe wavelengths, photoexcitation of electrons from the valence band (VB) into the conduction band (CB) results in depletion of electrons in the ground state (VB). This will cause an increase in transmission of the probe light, as reflected by a negative signal in our data. In the meantime, electrons generated in the CB or trap states may absorb the probe light, resulting in a decrease in transmission or a positive signal. Thus, the overall signal observed is composed of transient absorption and bleach, with their relative contribution determined by their absorption cross sections and relative electron populations in these states. If, for the same population, the excited state has a larger cross section than the ground state, a net transient absorption signal should be observed. However, if the excited state has a smaller cross section than the ground state, a net bleach signal should be observed. The situation may be more complicated when there are other states, e.g., trap states, involved. The trap states contribute to transient absorption, but their cross sections could be different from that of the CB. As the population in these states changes with time, the signal observed may appear as positive (absorption) or negative (bleach).

The bleach signal is simply due to a depletion of the ground state. The nature of the transient absorption signal is more complex and may be due to a number of possibilities, including free charge carriers (hot or thermalized), excitons, and trapped charge carriers. From previous studies of other semiconductor nanoparticles, it was found that transient absorption in the red−near-IR is dominated by deep trapped carriers on long time scales and at low excitation intensities.[40,44−46] On short (a few to a few tens of picoseconds) time scales, free carriers, excitons, or shallow trapped carriers can have a significant contribution to the transient absorption signal.[40,44,47−50] In some cases such as CdSe, CdS, and TiO_2, exciton−exciton annihilation becomes important at higher excitation intensities due to trap state saturation.[44] In Ag_2S, the power dependence of the observed amplitudes of the transient absorption and transient bleach signal appears to indicate trap state saturation, as will be explained later, however exciton−exciton annihilation does not seem to occur since the time constants of the observed decays do not change. Since hot electrons in the CB are expected to be extremely short-lived (<150 fs), their contribution to the transient absorption signal is assumed to be insignificant. The lack of excitonic features in the absorption spectra and the absence of detectable fluorescence indicate that excitons probably play an insignificant role in the observed dynamics. In addition, the excitonic state is usually very close in energy to the bottom of the CB, this state is expected to be in thermal equilibrium with the bottom of the CB. Therefore, the most likely assignment of the transient absorption signal is to electrons in the bottom of the CB (including the excitonic state) and in trap states. The cross section of these states will determine whether transient absorption or ground-state bleach will dominate the observed signal.

Modeling of Relaxation Dynamics. The observations described in the previous sections have led us to propose the following model for the excited-state kinetics of the Ag_2S nanoparticles. As shown in Figure 7A, photoexcitation at 390 nm initially populates the CB where electrons quickly (<150 fs) thermalize to the bottom of the band. At the same time, this excitation instantaneously creates a bleaching of the VB. The probe pulse can in principle be absorbed by electrons in any one of the states, depending on their absorption cross section at the probe wavelength. For the data presented, both transient absorption and transient bleach have been observed and their contribution to the overall signal depends on the relative absorption cross sections at the specific probe wavelengths and the population of the different states involved, which evolves in time. In general, the transient absorption signals arise from electrons in the CB, especially at short times, and from trap states. The contribution from trap states becomes more dominant at longer times as electrons relax from the CB to the trap states. The transient bleach signal is due to ground-state absorption, and its time evolution provides information about the recovery or recombination dynamics of charge carriers.

To gain further insight into the energy relaxation mechanism, a simple three-state kinetic scheme was used initially to model the observed dynamics. The three-state model was successful in modeling the observed data for sample GSH-1, but failed to fit the data for the other samples. The addition of a fourth state was then deemed necessary to account for the observed dynamics for all the samples. This model is not unique but provides a consistent description of the key dynamic features. Figure 7A displays the kinetic scheme used to model the

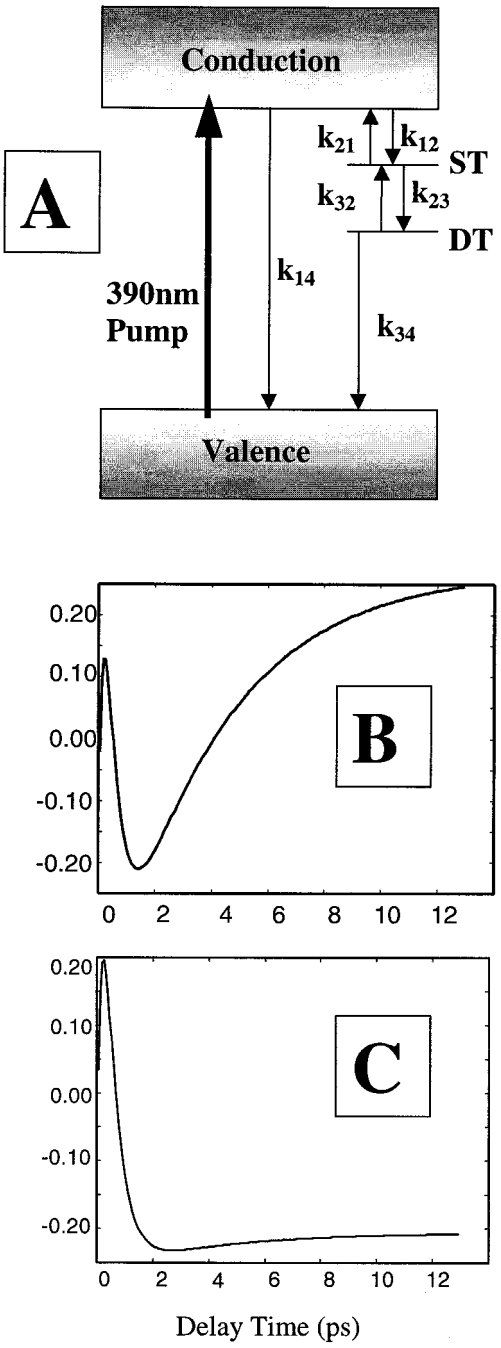

Figure 7. (A) Proposed energy level diagram for silver sulfide nanoparticles used in the kinetic modeling of the observed electron relaxation dynamics. ST is for shallow trap, and DT is for deep trap. (B) Representative dynamics result from kinetic modeling with large cross section of deep trap state. (C) Representative dynamics result from kinetic modeling with small cross section of deep trap state.

dynamic data. All samples were modeled using the same time constants, but with different contributions from the various states, reflecting their different absorption cross sections. The time constants were chosen from initial fitting of the experimental data and then iterating those values to generate the best fitting curves. The time constants used to generate curves which best fit the data are as follows: $k_{14} = 2.0 \times 10^{-3}$ ps^{-1}, $k_{12} = 2.0$ ps^{-1}, $k_{21} = 1.0 \times 10^{-1}$ ps^{-1}, $k_{23} = 2.5 \times 10^{-1}$ ps^{-1}, $k_{32} = 2.5 \times 10^{-2}$ ps^{-1}, and $k_{34} = 2.0 \times 10^{-3}$ ps^{-1}. The rate constant k_{12} corresponds to a time constant of 500 fs and accounts primarily for the trapping of electrons from the CB into shallow trap states. The rate constant k_{23} corresponds to a time constant of 4 ps and is primarily responsible for relaxation from shallow traps (ST) to deep traps (DT). Figure 7, parts B and C, display two examples of the curves generated using these kinetic parameters. Figure 7B shows the results when the following contributions from each of the states are made to the final signal: 44% CB, 4% ST, 39% DT, and 13% VB. Figure 7C is the resulting signal when the following contributions from each state are made: 59% CB, 6% ST, 17% DT, and 18%VB. These different contributions are assumed to reflect their difference in absorption cross sections at a particular probe wavelength. Based on this model, the difference in dynamics on long time scales between the GSH-1 sample and the other three samples can be explained by the different absorption cross sections of their deep trap states. This implies that the nature of the deep trap states in GSH-1 is different from that of the other samples, due to differences in the capping materials and in the ratios of silver:sulfide:capping materials.

Qualitatively the model works as follows. Following photoexcitation, the CB is populated and the VB is partially depleted. This should give rise to a transient absorption signal from the CB electrons and a bleach signal from the VB depletion, given the proper probe wavelength. Since initially a short-lived transient absorption signal was observed, the CB must have a larger cross section than the ground state, i.e., the transient absorption signal dominates over the bleach. As the CB electrons subsequently decay into ST states a transient bleach feature is observed, which indicates that the ST states have a smaller cross section than the CB and VB. As the electrons further relax from the ST to the DT states on longer time scales, the transient absorption becomes more dominant again. This suggests a larger cross section of the DT states than the ST states and VB.

As the excitation intensity is increased, a buildup of electrons may occur in the CB due to trap-state saturation. The recovery of the ground state may become slower since trap-state saturation will effectively block some of the relaxation pathways that are otherwise mediated by the trap states. These combined effects of population buildup in the CB and delayed recovery of the ground state will lead to more dominant transient absorption over bleach, which is what has been observed for all the four samples studied. Quantitative modeling indicates that it is the saturation of the shallow trap states that is most effective in generating the power dependence. This is probably because the relaxation from CB to ST is much faster than that from ST to DT and high intensity excitation leads to accumulation of electrons in ST states, and thereby saturation, more easily than in DT states. Evidence of trap-state saturation at high intensities has been found previously for CdS nanoparticles.[44]

The above kinetic model seems to suggest that the different dynamics between GSH-1 and the other three samples can be explained by their difference in absorption cross sections of the deep traps. To gain a better understanding of the possible cause for the difference in deep trap states, we examine the different samples in some more detail. Both GSH-1 and Cys-1 samples have higher silver:sulfide ratios (1:0.5) than GSH-2 and Cys-2 (1:1). GSH-1 and Cys-1 also have a greater amount of capping material than GSH-2 and Cys-2. If particles with similar capping materials but different silver:sulfide ratios are compared, as in the case of Cys-1 and Cys-2, their dynamics appear identical. Thus, it appears that the stoichiometric ratio alone does not affect the deep trap cross section or kinetics. However, when the two GSH samples, with the same capping material but different silver:sulfide ratios, are compared, a clear difference is observed in their dynamics. This seems to suggest a connection between the stoichiometric ratio and the nature of the deep trap states.

On the other hand, when two samples with similar stoichiometric ratios but different capping materials are compared, e.g., Cys-2 and GSH-2, there appears to be no difference in their dynamics, lending to the notion that the deep trap states are not significantly affected by the capping material. However, comparison between Cys-1 and GSH-1 shows a distinct difference in their dynamics, which seems to suggest the capping material does influence the deep trap states. Therefore, there are two possible ways to rationalize all the data obtained. One is to suggest that the capping material affects the deep trap states only when the stoichiometric ratio between the silver:sulfide is high and the amount of capping material is large. Another possible rationalization is that the stoichiometric ratio between the silver:sulfide affects the deep trap states only when glutathione is the capping material. The effect most likely reflects changes in the energetics of deep trap states. Further investigation is necessary to better understand the difference between the different samples.

Conclusions

To summarize, Ag_2S colloidal nanoparticles capped with cysteine or glutathione have been prepared using a new synthetic method. Ultrafast dynamics of photoinduced electrons in these nanoparticles have been measured using femtosecond transient absorption/bleach spectroscopy. In most cases, the early time transient profiles feature a pulse-width limited rise followed by a fast decay (750 fs) and a slower rise (4.5 ps). On longer time scales, a slow decay for Cys-1, Cys-2, and GSH-2, or a slow rise in the case of GSH-1, with time constant of >1 ns has been observed. The signal contains contribution from both transient absorption and transient bleach.

The simple four-state kinetic model developed has been used to successfully explain the key features of the observed dynamics. The model suggests that initial photoexcitation populates the CB and depletes the VB in <150 fs, with thermalization of electrons to the bottom of the CB occurring on a similar time scale. The thermalized electrons are first trapped in shallow trap states with a time constant of about 500 fs and then further trapped into deep traps with a time constant of 4 ps. The deep trapped electrons finally recombine with the holes with a time constant of >1 ns. Difference in absorption cross sections of deep trap states, which depends on the capping material and stoichiometric ratio of silver:sulfide:capping material, has been suggested to be the cause for the difference in dynamics between the GSH-1 sample and other samples. The dependence of dynamics on excitation intensity observed has been attributed to shallow trap state saturation at high intensities.

Acknowledgment. M.C.B. and J.Z.Z. acknowledge financial support from Petroleum Research Fund administered by the American Chemical Society, Collaborative UC Los Alamos Research Fund (CULAR), and the Faculty Research Fund of UC Santa Cruz. R.K.M. and L.N. acknowledge the financial support of a CULAR grant and from UCR Academic Senate. The authors thank Dr. Jun Liu and Prof. Zhong-lin Wang for their help in carrying out HRTEM measurements to characterize the particle size.

References and Notes

(1) Mehra, R. K.; Winge, D. R. *J. Cell. Biochem.* **1991**, *45*, 30.

(2) Winge, D. R.; Mehra, R. K. *Int. Rev. Exp. Pathol.* **1990**, *31*, 47.

(3) Mehra, R. K.; Tarbet, E. B.; Gray, W. R.; Winge, D. R. *Proc. Natl. Acad. Sci. U.S.A.* **1988**, *85*, 8815.

(4) Dameron, C. T.; Reese, R. N.; Mehra, R. K.; Kortan, P. J.; Carrol, M. L.; Steigerwald, M. L.; Brus, L. E.; Winge, D. R. *Nature* **1989**, *338*, 596.

(5) Mehra, R. K.; Mulchandani, P.; Hunter, T. C. *Biochem. Biophys. Res. Commun.* **1994**, *200*, 1193.

(6) Barbas, J.; Santhanagopalan, V.; Blaszczynski, M.; Ellis, W. R.; Winge, D. R. *J. Inorg. Biochem.* **1992**, *48*, 95.

(7) Zenk, M. H. *Gene* **1996**, *179*, 21.

(8) Dameron, C. T.; Winge, D. R. *Inorg. Chem.* **1990**, *29*, 1343.

(9) Bae, W.; Abdullah, R.; Henderson, D.; Mehra, R. K. *Biochem. Biophys. Res. Commun.* **1997**, *237*, 16.

(10) Bae, W.; Mehra, R. K. *J. Inorg. Biochem.* **1997**, *68*, 201.

(11) Bae, W.; Mehra, R. K. *J. Inorg. Biochem.* **1998**, *69*, 33.

(12) Bae, W.; Mehra, R. K. *J. Inorg. Biochem.* **1998**, *70*, 125.

(13) Nguyen, L.; Kho, R.; Bae, W.; Mehra, R. K. *Chemosphere* **1999**, *38*, 155.

(14) Yanagida, S.; Kawakami, H.; Midori, Y.; Kizumoto, H.; Pac, C.; Wada, Y. S. *Bull. Chem. Soc. Jpn.* **1995**, *68*, 1811.

(15) Motte, L.; Billoudet, F.; Pileni, M. P. *J. Mater. Sci.* **1996**, *31*, 38.

(16) Lawless, D.; Kapoor, S.; Meisel, D. *J. Phys. Chem.* **1995**, *99*, 10329.

(17) Alivisatos, A. P., Bruchez, M., Jr.; Moronne, M.; Gin, P.; Weiss, S. *Science* **1998**, *281*, 2013.

(18) Chan, W. C. W.; Nie, S. *Science* **1998**, *281*, 2016.

(19) Motte, L.; Pileni, M. P. *J. Phys. Chem. B* **1998**, *102*, 4104.

(20) Pileni, M. P.; Motte, L.; Billoudet, F.; Mahrt, J.; Willig, F. *Mater. Lett.* **1997**, *31*, 255.

(21) Kitova, S.; Eneva, J.; Panov, A.; Haefke, H. *J. Imag. Sci. Technol.* **1994**, *38*, 484.

(22) Heath, J. R.; Shiang, J. J. *Chem. Soc. Rev.* **1998**, *27*, 65.

(23) Henglein, A. *Chem. Rev.* **1989**, *89*, 1861.

(24) Alivisatos, A. P. *Science* **1996**, *271*, 933.

(25) Alivisatos, A. P. *J. Phys. Chem.* **1996**, *100*, 13226.

(26) Bawendi, M. G.; Steigerwald, M. L.; Brus, L. E. *Annu. Rev. Phys. Chem.* **1990**, *41*, 477.

(27) Bawendi, M. G.; Wilson, W. L.; Rothberg, L.; Carroll, P. J.; Jedju, T. M.; Steigerwald, M. L.; Brus, L. E. *Phys. Rev. Lett.* **1990**, *65*, 1623.

(28) Zhang, J. Z. *Acc. Chem. Res.* **1997**, *30*, 423.

(29) Tennakone, K.; Kumara, G. R.; Kumarasinghe, A.; Wijayantha, K.; Sirimanne, P. *Semicond. Sci. Technol.* **1995**, *10*, 1689.

(30) Smestad, G.; Bignozzi, C.; Argazzi, R. *Sol. Energy Mater. Sol. Cells* **1994**, *32*, 259.

(31) O'Regan, B.; Grätzel, M. *Nature* **1991**, *353*, 737.

(32) Nazeeruddin, M. K.; Kay, A.; Rodicio, I.; Humphry-Baker, R.; Muller, E.; Liska, P.; Vlachopoulos, N.; Gratzel, M. *J. Am. Chem. Soc.* **1993**, *115*, 6382.

(33) Kay, A.; Grätzel, M. *J. Phys. Chem.* **1993**, *97*, 6272.

(34) Cherepy, N. J.; Liston, D.; Lovejoy, J.; Deng, H.; Zhang, J. Z. *J. Phys. Chem. B* **1997**, *102*, 770.

(35) Ellingson, R. J.; Asbury, J. B.; Ferrere, S.; Ghosh, H. N.; Sprague, J. R.; Lian, T.; Nozik, A. J. *J. Phys. Chem. B* **1998**, *102*, 6455.

(36) Ghosh, H. N.; Asbury, J. B.; Lian, T. *J. Phys. Chem. B* **1998**, *102*, 6482.

(37) James, T. H. *The Theory of the Photographic Process*, 4th ed.; MacMillan Publishing Co: New York, 1977.

(38) Hamilton, J. F. *Adv. Phys.* **1988**, *37*, 359.

(39) Sahyun, M. R. V.; Sharma, D. K.; Serpone, N. *J. Imag. Sci. Technol.* **1995**, *39*, 377.

(40) Brelle, M. C.; Zhang, J. Z. *J. Chem. Phys.* **1998**, *108*, 3119.

(41) Zhang, J. Z.; O'Neil, R. H.; Roberti, T. W. *J. Phys. Chem.* **1994**, *98*, 3859.

(42) von der Oster, M.; Landolt-Bornstein, 1982; Vol. 172, p 156.

(43) Sengupta, A.; Jiang, B.; Mandal, K. C.; Zhang, J. Z. *J. Phys. Chem. B* **1999**, *103*, 3128.

(44) Roberti, T. W.; Cherepy, N. J.; Zhang, J. Z. *J. Chem. Phys.* **1997**, *108*, 2143.

(45) O'Neil, M.; Marohn, J.; McLendon, G. *Chem. Phys. Lett.* **1990**, *168*, 208.

(46) Klimov, V.; Haring-Bolivar, P.; Kurz, H. *Phys. Rev. B* **1996**, *53*, 1463.

(47) Klimov, V.; Haring-Bolivar, P.; Kurz, H.; Karavanskii, V. *Superlattices Microstruct.* **1996**, *20*, 395.

(48) Bowman, R. M.; Skinner, D. E.; Colombo, D. P., Jr.; Cavaleri, J. J. *J. Phys. Chem.* **1995**, *99*, 7853.

(49) Alfano, R. R.; Shum, K.; Wang, W. B.; Jones, K. M. *Phys. Rev. Lett.* **1992**, *68*, 3904.

(50) Logunov, S.; Green, T.; Marguet, S.; El-Sayed, M. A. *J. Phys. Chem. A* **1998**, *102*, 5652.